Spatial and Seasonal Controls on Eddy Subduction in the Southern Ocean

Michael L. Chen[1], Oscar Schofield[1]

[1]Department of Marine and Coastal Sciences, Rutgers University, New Brunswick, NJ, USA

Corresponding author: Oscar Schofield (oscar@marine.rutgers.edu)

Key Points:

- Eddy subduction in the Southern Ocean is observed as subsurface anomalies in spice and oxygen measured by autonomous profiling floats
- Spatial distribution is controlled by weak stratification and strong lateral buoyancy gradients, diagnosed using satellite altimetry
- Bio-optical proxies suggest that eddy subduction is most active in spring/early summer, driven by weak vertical stratification

Abstract

Carbon export driven by submesoscale, eddy-associated vertical velocities ("eddy subduction") remains understudied, leaving a gap in our understanding of ocean carbon sequestration. Here, we assess mechanisms controlling eddy subduction's spatial and seasonal patterns using 15 years of observations from BGC-Argo floats in the Southern Ocean. We identify signatures of eddy subduction as subsurface anomalies in temperature-salinity and oxygen. The anomalies' spatial distribution is concentrated near weakly stratified areas and regions with strong lateral buoyancy gradients diagnosed from satellite altimetry, particularly in the Antarctic Circumpolar Current's standing meanders. Meanwhile, vertical stratification drives seasonal variability. Bio-optical proxies associated with subsurface anomalies (such as the Chlorophyll *a* to particulate backscatter ratio: Chl/b_{bp}), indicate that eddy subduction is most active in the spring and early summer, with freshly exported material associated with seasonally weak vertical stratification. Climate change is increasing ocean stratification globally, which may weaken eddy subduction's carbon export potential.

Plain Language Summary

Oceans play an important role in global climate by soaking up and sequestering atmospheric carbon dioxide. Photosynthetic activity at the surface turns carbon dioxide into organic carbon, and if this carbon leaves the surface to the deep ocean, it can be locked away from the atmosphere. One way this occurs is through the physical circulation associated with swirling eddies, which can rapidly transport carbon-rich surface waters and "inject" them into deep waters. However, we still don't fully understand the seasonal timing of this process, or what drives its spatial distribution. We investigated this in the Southern Ocean, which is very important to global climate, using data collected by drifting robots. We find that this process is the most active in regions where eddies drive strong surface stirring, and during the spring, when weak stratification allows injections to penetrate deep into the ocean. Because this process is poorly represented in climate models, these findings will improve our understanding of how the ocean absorbs carbon.

1 Introduction

Oceans play a critical role in regulating global climate by sequestering carbon from the atmosphere (Gruber et al., 2009). A key driver of this is the biological pump, a suite of processes that exports carbon from the ocean's surface to the interior, where it can be sequestered for years to centuries. Recent modeling suggests that the biological pump keeps 1,300 Pg C sequestered from the atmosphere (Nowicki et al., 2022). The best understood mechanism is the biological gravitational pump, or the sinking of large particles and aggregates out of the euphotic zone, which is estimated to comprise about 70% of global carbon export (Boyd et al., 2019; Nowicki et al., 2022). However, contributions by other mechanisms of carbon export are increasingly being recognized (Boyd et al., 2019). These include biological mechanisms such as transport by vertically migrating mesopelagic organisms (Bianchi et al., 2013), and physical processes such as carbon detrainment from shoaling mixed layers (the "mixed-layer pump"; Dall'Olmo et al., 2016; Lacour et al., 2019), large-scale water mass subduction (the "subduction pump"; Levy et

al., 2013), and submesoscale vertical velocities associated with frontal boundaries and eddies (the "eddy subduction pump", or "ESP"; Omand et al., 2015; Resplandy et al., 2019).

Among these, eddy subduction (henceforth, also “subduction”) remains understudied and under-observed due to the challenges of observing these submesoscale processes. In recent decades, submesoscale physics has emerged as a key driver of vertical biogeochemical transport. Advances in high-resolution numerical modeling have revealed a dynamic eddy field at horizontal scales of O(1-10) m, associated with strong, ageostrophic vertical velocities reaching up to 100 m day^{-1}. These evolve on timescales of O(1) days with a vertical extension of O(100) m, and strongly contribute to vertical tracer variability in models (Balwada et al., 2018; Capet et al., 2008; Klein & Lapeyre, 2009; Lapeyre & Klein, 2006; Lévy et al., 2012; Mahadevan & Tandon, 2006; Rosso et al., 2014). Mechanisms energizing these submesoscale flows include surface frontogenesis associated with dynamic strain fields (Held et al., 1995; Lapeyre & Klein, 2006; Rosso et al., 2015), as well as baroclinic instabilities within the mixed layer (“mixed layer instabilities”), which extract potential energy stored in lateral buoyancy gradients and deep mixed layers (Boccaletti et al., 2007; Callies et al., 2015, 2016; Erickson & Thompson, 2018); observations of seasonality in some regions have shown peak velocities associated with deep winter mixed layers (Buckingham et al., 2016; Callies et al., 2015; Thompson et al., 2016).

If downward vertical motions coincide with the presence of particulate carbon in the surface ocean, carbon export can occur. During phytoplankton blooms, models and observations show that filaments of carbon-rich surface waters can be injected to depth along eddy peripheries. Once subducted, these parcels of water retain tracer signatures of their surface origins, including elevated oxygen and surface-like temperature-salinity (Davies et al., 2019; Omand et al., 2015). Recently, Llort et al. (2018) developed an algorithm to detect eddy subduction events in BGC-Argo float profiles by identifying subsurface anomalies in apparent oxygen utilization (AOU) and spice (a temperature-salinity variable that reflects isopycnal water-mass contrasts; McDougall & Krzysik, 2015), often co-located with elevated particulate organic carbon (POC). This approach has been applied to identify eddy subduction in energetic regions such as the Southern Ocean (Lacour et al., 2023; Llort et al., 2018), the North Atlantic (Johnson & Omand, 2021) and the Kuroshio Extension (Chen et al., 2021). Estimates of the eddy subduction pump’s overall contribution to carbon export vary widely, ranging from being responsible for up to 50% of exported POC during spring blooms, to as little as <5% (Davies et al., 2019; Llort et al., 2018; Omand et al., 2015; Resplandy et al., 2019; Stukel & Ducklow, 2017).

Eddy subduction’s seasonal variability and the mechanisms responsible remain unresolved, representing a major gap in carbon export estimates (Nowicki et al., 2022). Previous observational studies have largely addressed seasonality through the timing of detecting subsurface anomalies, with mixed findings (Chen et al., 2021; A. R. Johnson & Omand, 2021; Lacour et al., 2023; Llort et al., 2018). However, the timing of these observations don’t necessarily reflect the timing of subduction itself, as the anomalies used for detection may have persisted at depth for months after subduction actually occurred (Johnson & Omand, 2021).

Here, we provide observational evidence from BGC-Argo floats in the Southern Ocean and integrate bio-optical proxies to assess eddy subduction’s seasonality and spatial distribution, and link it to physical drivers. We identify a seasonal cycle peaking in the austral spring, associated with weak vertical stratification. Integrating satellite altimetry, we find that strong lateral

buoyancy gradients, along with weak stratification, shape eddy subduction's spatial distribution, but not its seasonality. This work provides an important step towards understanding physical contributions to carbon export in the Southern Ocean, a globally important region in ocean carbon cycling.

2 Data and Methods

2.1 Float Data

BGC-Argo float data are from the Southern Ocean Carbon and Climate Observations and Modeling (SOCCOM) program. Floats conduct 2000 m vertical profiles every 10 days, and drift at a parking depth of 1000 m. Vertical sampling frequency varies between the two float types in this dataset: Navis floats sample every 2 m in the upper 1000 m, while APEX floats sample less frequently, with resolution decreasing with depth. Sampling schemes are described in Johnson et al. (2017), as well as processing of bio-optical parameters, including optical backscatter at 700 nm (b_{bp}), which is used to derive POC, and chlorophyll *a* fluorescence, which is used to derive chlorophyll *a* concentrations (Chl). Quality control procedures for all other variables are described in Maurer et al. (2021). Only data flagged as "good" were used.

Variables such as conservative temperature (CT) and absolute salinity (S_A) were derived using the Thermodynamic Equation of Seawater 2010 (TEOS-10; McDougall & Barker, 2011), and spice was calculated as a function of CT and S_A, following McDougall & Krzysik, 2015. AOU was calculated as ($AOU = O_2^{sat} - O_2^{obs}$), where O_2^{sat} is the oxygen saturation concentration calculated using the coefficients of Garcia & Gordon (1992, 1993), and O_2^{obs} is the observed dissolved oxygen concentration. Mixed layer depth was defined using a density difference threshold of 0.05 kg m^{-3} from the surface, and buoyancy frequency squared (N^2) was calculated using TEOS-10.

2.2 Eddy Subduction Anomaly Detection

We identified eddy subduction anomalies in float profiles using an algorithm adapted from Chen et al. (2021) and Llort et al. (2018). An example is shown in Figure 1, detected on the periphery of a mesoscale eddy (Figure 1a). We considered profiles between 30°S and 65°S, and discarded profiles with surface salinity > 35 psu, following Llort et al. (2018). We also only considered profiles where the median spice value in the mixed layer was lower than that at 600 m, as increasing spice with depth in the upper 1000m is characteristic of Southern Ocean waters (Tailleux, 2021). Navis floats were down-sampled by selecting data at APEX sampling depths, allowing for comparable vertical resolution. Profiles were then vertically smoothed with a 3-bin rolling median. The total dataset contained 9,354 profiles collected from February 2008 through August 2023.

For each smoothed profile, we identified co-occurring peaks in spice and AOU between the MLD and 600 m depth (defined as relative minima found within 30 meters of each other, at depths h_{spice} and h_{AOU}; Figure 1b,c). We then defined reference profiles to simulate "background", ambient values in the absence of subduction (orange lines, Figure 1b,c). An initial guess for the reference profile is defined as the straight line in between the maximum values above and below each peak (within 100 m in either direction), following Chen et al., 2021. If the

line intersects with the observed profile, the top and bottom boundaries of this initial guess are iteratively adjusted inwards (towards the peak) until the profiles no longer intersect (Supporting Information Figure S1). We then calculated the difference between the observed value and the calculated reference value at h_{spice} and h_{AOU}, yielding Δ_{spice} and Δ_{AOU}, respectively (Figure 1b,c). Peaks were classified as eddy subduction pump anomalies ("ESP anomalies") if $\Delta_{spice} < -0.05$ kg/m^3 and $\Delta_{AOU} < -8$ µmol/kg, following Llort et al. (2018). The anomaly depth was defined at h_{AOU}, and the vertical extent of the anomaly (H) was defined as the extent of the reference profile for AOU. We discarded anomalies found within 100 m of the MLD in order to avoid misidentifying detrainment from shoaling mixed layers (Lacour et al., 2019).

In order to quantify subduction-driven values associated with an anomaly (e.g. POC and Chl/b_{bp}), we first integrated the observed quantities over the span of H (e.g. POC_{ESP_total} and Chl/b_{bp_total}). We then estimated the ambient values (i.e. in the absence of subduction) by integrating through reference profiles, defined as the straight line between the observed values at the top and bottom of H (e.g. $POC_{ambient}$ and Chl/$b_{bp\_ambient}$: hatched regions in Figure 1d,e). We subtracted ambient values from total values, yielding "subduction-driven" integrated values (e.g. POC_{ESP} and Chl/b_{bp_ESP}: green shaded regions in Figure 1d,e). Finally, we normalized these by H to yield depth-averaged, subduction-driven quantities within anomalies (e.g. POC_{ESP_avg} and Chl/$b_{bp\_ESP\_avg}$), which are the principal values discussed hereafter.

2.3 Satellite Data

Finite-size Lyapunov Exponents (FSLEs) were downloaded from AVISO+. FSLEs describe stretching and compression by quantifying the exponential rate of separation (λ) of neighboring particles advected in a flow field: $\lambda(d_0, d_f) = \frac{1}{t} log(\frac{d_f}{d_0})$, where d_0 and d_f are the initial and final distances between the particles, respectively, and t is the time it takes for the particles to reach d_f (d'Ovidio et al., 2004). The AVISO+ product uses daily, altimetry-derived geostrophic velocity fields to advect particles backward-in-time, so FSLEs are negative, with stronger negative values indicating stronger stretching; these FSLE ridges indicate transport barriers and are preferentially located between eddy cores (Siegelman et al., 2020a; also demonstrated here in Figure 1a).

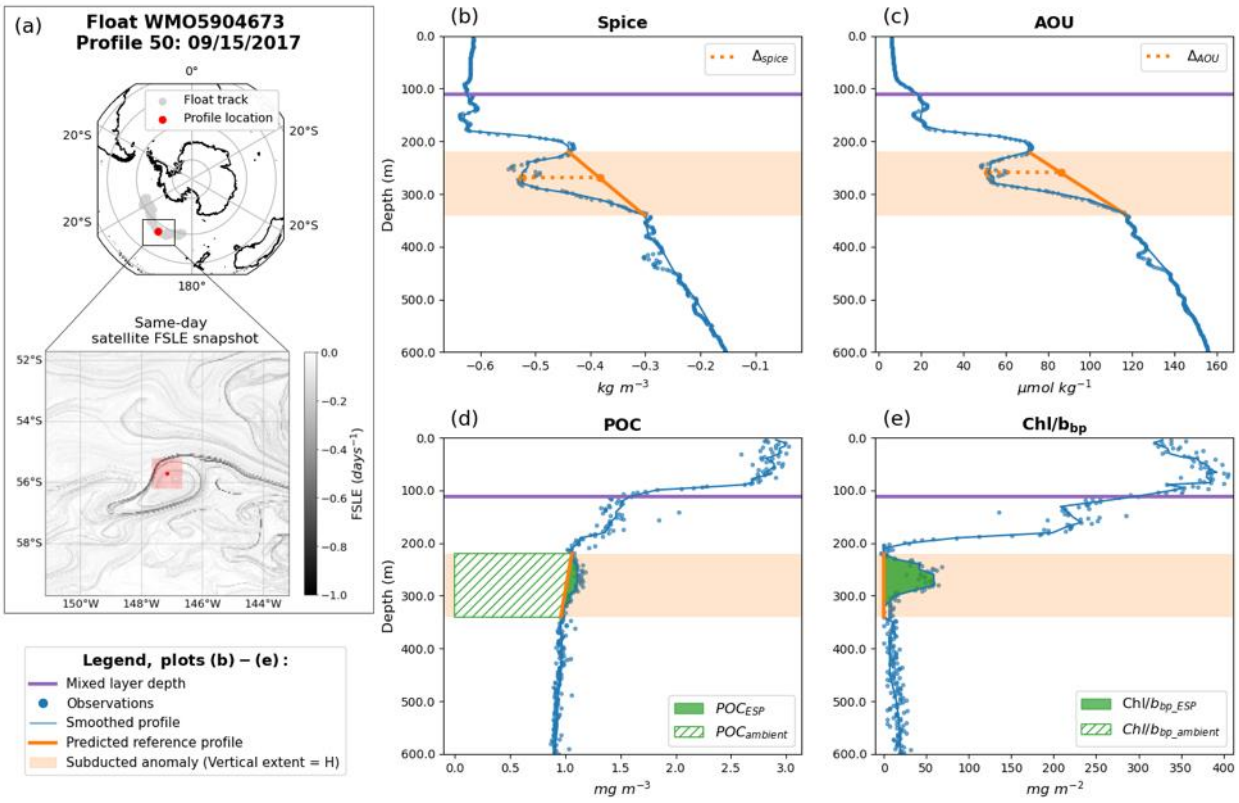

Figure 1. Example of an eddy subduction anomaly detected in a float profile. **(a)** Map depicting float track and profile location (red circle). Inset shows the same-day surface FSLE field. Red circle = profile location. Shaded red box = the 1°x1° area used to retrieve the strongest FSLE in the profile's vicinity. The float's vertical profiles are shown in **(b-d),** with the MLD indicated by a purple line. Blue lines depict smoothed profiles. The shaded orange band indicates H, the vertical extent of the subduction anomaly. **(b)** Spice profile. Dotted orange line shows Δ_{spice} at depth h_{spice}, or the difference between the observed value and the calculated reference value (orange circles). The reference profile is shown by the orange line. (**c)** AOU profile, with reference profile and Δ_{AOU}, similar to the spice profile. **(d)** POC profile. Shaded green region: POC_{ESP}, the integrated quantity of subduction-driven POC. Hatched region: $POC_{ambient}$, the subtracted, integrated quantity of ambient POC. (**e**) Chl/b_{bp} ratio profile. Shaded green area: Chl/b_{bp_ESP}, similar to POC. Hatched region: $Chl/b_{bp\_ambient}$, not visible because values are roughly 0.

3 Results and Discussion

3.1 Spatial Distribution of Eddy Subduction

The BGC-Argo dataset provides full, basin-wide spatial coverage of the Southern Ocean over 15 years. We find eddy subduction anomalies in 4.4% of profiles, defined as coherent, negative mesopelagic anomalies in spice and AOU (Figure 1b,c), frequently associated with positive anomalies in bio-optical parameters (Figure 1d,e). These anomalies are spatially concentrated around the Polar Front and Antarctic Circumpolar Current (ACC), consistent with Llort et al. (2018) (Figure 2a). However, their circumpolar distribution is uneven, with most detected in the

ACC's standing meander regions: the Eastern Pacific Rise, the Kerguelen, Crozet, and Campbell Plateaus, and the Drake Passage. These regions are known for enhanced eddy kinetic energy (EKE) and vertical exchange (Dove et al., 2022), as the vigorous flow of the ACC is diverted by underwater topography, generating mesoscale eddies that strain surface density fields and create strong lateral buoyancy gradients. This frontogenesis can subsequently energize vigorous submesoscale motions (Rosso et al., 2015).

To better assess spatial distribution, we use altimetry-derived FSLEs, a powerful Lagrangian diagnostic of submesoscale activity. FSLEs are elevated within the ACC's standing meanders (Dove et al., 2022), and strong FSLEs have been shown to be co-located with strong, deep-reaching submesoscale lateral buoyancy gradients and the intense vertical velocities associated with them (Siegelman, et al., 2020a,b). Thus, to assess whether a given float profile was in the vicinity of submesoscale fronts, we matched each profile with its same-day satellite FSLE field and identified the strongest FSLE within the surrounding 1°x1° area (e.g. within the red square in Figure 1a). These matchups are displayed in Figure 2b and clearly show the ACC's standing meanders as hotspots of submesoscale activity (i.e. strong FSLEs), largely congruent with the distribution of eddy subduction anomalies.

However, some groups of anomalies are detected in comparatively quiescent regions in between the standing meanders, such as 60-120°W and 150-180°W (Figure 2a,b). Vertical stratification strength is another mechanism known to influence submesoscale activity, with weak stratification allowing deeper penetration of vertical velocities (Callies et al., 2016; Erickson & Thompson, 2018). Although stratification shows a less dramatic spatial pattern than FSLEs, many float profiles in these regions have notably weak stratification (yellow colors in Figure 2c), suggesting that this could also influence eddy subduction's spatial distribution. These mechanistic relationships will be further explored statistically in Section 3.3.

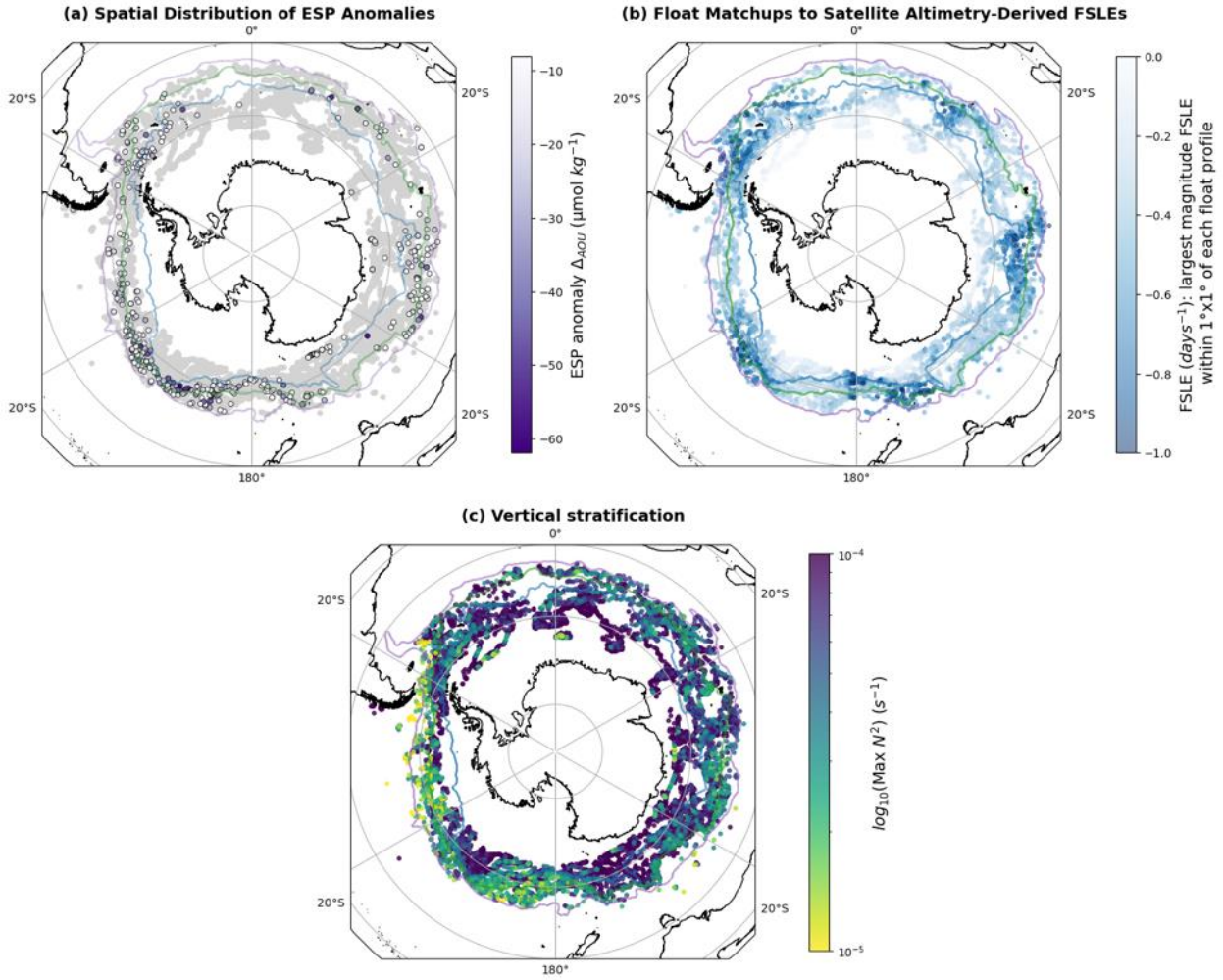

Figure 2. Maps of the float dataset. Colored lines indicate front locations as defined by mean dynamic topography from satellite altimetry (Park & Durand, 2019): purple=Subantarctic Front (SAF); green=Polar Front (PF); blue=Southern ACC Front (SACCF). **(a)** Locations of eddy subduction anomalies across the Southern Ocean. Gray circles indicate all float profiles considered in the analysis. Purple-scale colored circles indicate detected ESP anomalies, colored by the magnitude of Δ_{AOU}. **(b)** Spatial distribution of FSLE magnitudes, a proxy for the strength of lateral buoyancy gradients. Each point is a satellite matchup to a float profile, showing the strongest FSLE within 1°x1° of each profile. (**c)** Spatial distribution of vertical stratification in each float profile, measured as maximum N^2, and displayed on a log-scale. The colorscale maximum is limited to 10^{-4} (roughly the median of the maximum N^2 distribution; see Figure 4d) to emphasize variation in the lower half of the distribution.

3.2 Seasonality of Eddy Subduction

We detect subduction anomalies more frequently during summer months (Figure 3a). However, the timing of detection does not necessarily indicate the timing of subduction, as the coarse spatial and temporal resolution of BGC-Argo floats cannot provide Lagrangian tracking of individual subduction events as they evolve. Instead, our method can only identify subsurface

tracer anomalies after subduction occurs, and these anomalies may persist for months at depth afterwards (Johnson & Omand, 2021).

To assess the timing of subduction, we look at other proxies. A useful metric is the Chl/b_{bp} ratio, or the ratio of chlorophyll *a* to particulate backscatter. At the surface, this ratio reflects phytoplankton photophysiology and community composition (Barbieux et al., 2018; Cetinić et al., 2015; Rembauville et al., 2017). However, beneath the mixed layer, it can be a proxy for the freshness of exported material; in the days after particulate material leaves the mixed layer, Chl/b_{bp} decays by a power law as phytoplankton and their pigments degrade (Lacour et al., 2019). Accordingly, this ratio is high within the mixed layer and over an order of magnitude lower in the mesopelagic (Supporting Information Figure S2). Within subduction anomalies, Chl/$b_{bp\_ESP\_avg}$ is frequently elevated relative to ambient mesopelagic waters, indicating freshly subducted phytoplankton biomass (Figure 1e). It also has a notable seasonal cycle, with the highest values, indicating the most freshly subducted material, occurring during the spring and early summer (Figure 3b). AOU within subducted anomalies ($AOU_{\_ESP\_avg}$) shows a similar seasonality, with the most negative values occurring during the spring (Figure 3c), indicating less respiration, or "aging", has occurred.

By comparison, the seasonal cycle of eddy-subducted POC ($POC_{\_ESP\_avg}$; Figure 1d) is slightly delayed, with summer-detected anomalies carrying the highest POC content (Figure 3d). This suggests that despite high Chl/$b_{bp\_ESP\_avg}$ values, springtime subduction events may not necessarily export large amounts of biomass. However, most detected anomalies carry little excess POC relative to ambient waters, resulting in little seasonality when averaging (Figure 3d). Importantly, these seasonal cycles are distinct from those of ambient values in the mesopelagic, which are influenced by other processes such as gravitational sinking of large particles. Ambient values of both POC and Chl/b_{bp} show strong seasonality beneath the mixed layer, peaking in mid-late summer (Supporting Information Figure S3). Spike analyses following Briggs et al. (2011) indicate that this is likely driven by large particle sinking, which is also highest during mid-late summer (Supporting Information Figure S4).

The metrics here provide a novel, qualitative overview of previously unresolved seasonality in eddy subduction, suggesting it is most active in the spring and early summer. However, fully understanding its timing will require high-resolution sampling to dissect the physical and biogeochemical processes that contribute to the destruction of coherent tracer anomalies over time; for example, turbulent mixing will affect all variables discussed here, while respiration will transform biogeochemical tracers such as AOU and POC. The Chl/b_{bp} ratio is additionally subject to chlorophyll pigment degradation. Notably, anomalies in spice should only be dissipated by turbulent mixing, and $spice_{\_ESP\_avg}$ does not show a seasonal cycle (Figure 3e), suggesting that the relative roles of physics vs respiration in dissipating subducted features need to be further untangled. However, the observed seasonality is informative in diagnosing mechanisms, discussed next.

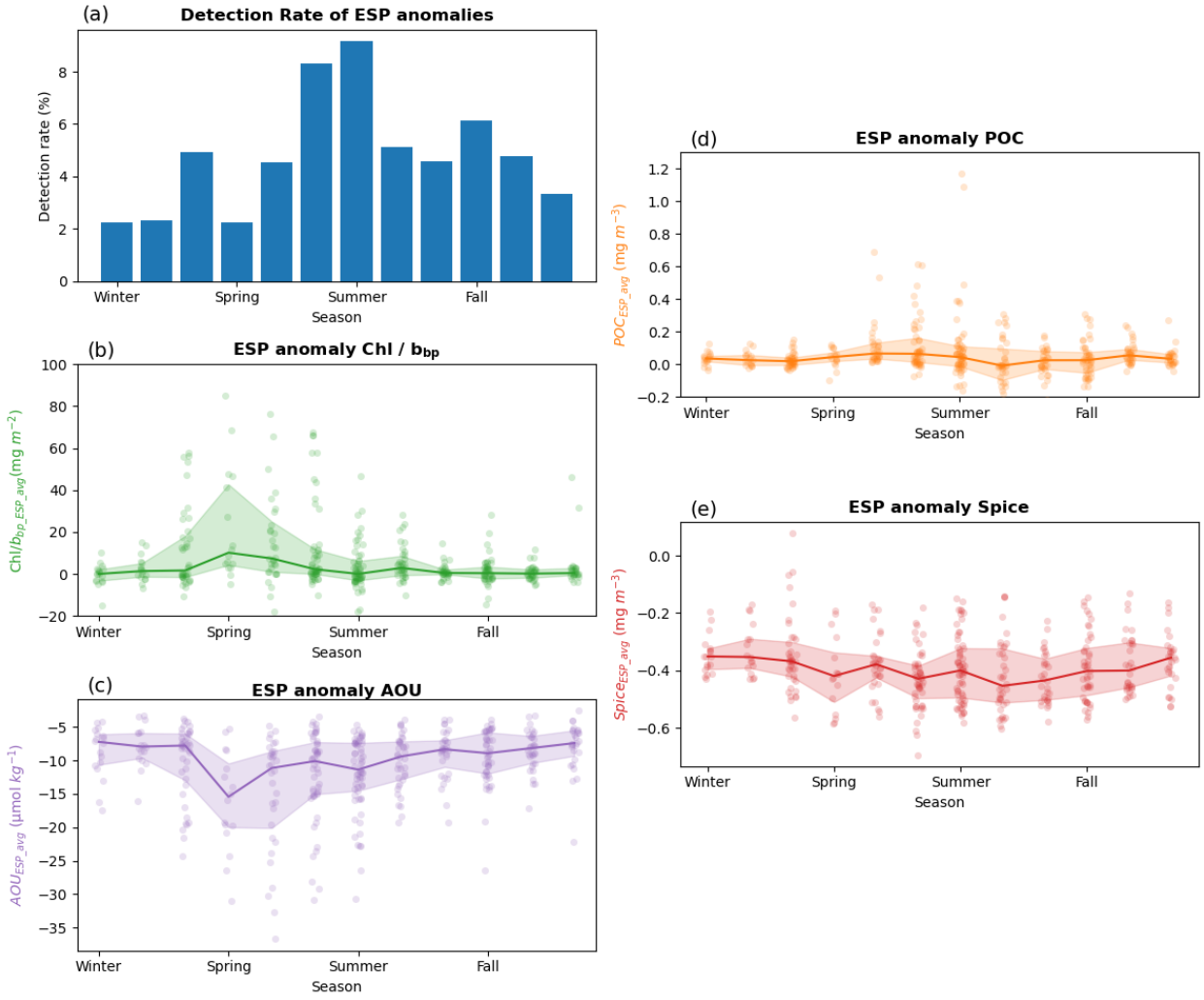

Figure 3. Seasonal patterns across observed ESP anomalies. X-axis ticks correspond to [June, Sept, Dec, Mar]. **(a)** Detection rate of ESP anomalies per month, normalized by the total number of profiles per month. Plots **(b-e)** show seasonality of depth-averaged properties within ESP anomalies, with ambient values subtracted. Line plots depict medians, with shaded regions indicating interquartile ranges. Overlain strip plots show individual data points. **(b)** $POC_{\_ESP\_avg}$, **(c)** $Chl/b_{bp\_ESP\_avg}$, **(d)** $AOU_{\_ESP\_avg}$, **(e)** $spice_{\_ESP\_avg}$. Axis limits in **(b)** and **(d)** display 98% of data points.

3.3 Physical and Biological Mechanisms Controlling Spatial and Seasonal Patterns

Multiple physical and biological processes are required for eddy subduction. Physically, the strength of submesoscale overturning circulations scales with strong lateral buoyancy gradients and deep mixed layers (Fox-Kemper et al., 2008). Additionally, weak vertical stratification allows these velocities to penetrate deeper into the interior (Callies et al., 2016; Erickson & Thompson, 2018). Finally, POC must be available at the ocean's surface for export. Examining seasonal cycles in these variables, spring/early summer emerges as a period conducive to eddy subduction across the Southern Ocean, with an overlap of deep mixed layers, weak vertical

stratification (defined as maximum N^2), and increasing POC in the mixed layer (Figure 4a). This aligns with the seasonality discussed in Section 3.2. Interestingly, altimetry-derived FSLEs, an indicator of lateral buoyancy gradients (Siegelman et al., 2020a), do not show a seasonal cycle here (Figure 4b), suggesting that lateral buoyancy gradients in this region may not drive the eddy subduction's seasonality.

Statistical distributions of float profiles provide further insights into these mechanisms. Profiles with subduction anomalies are shifted towards higher surface POC content (Figure 4c), demonstrating that carbon must be available to be exported. Similarly, profiles with subduction anomalies are shifted towards more weakly stratified water columns (Figure 4d). Profiles with anomalies in the top quartile of Chl/$b_{bp\_ESP\_avg}$ values, likely the most recently subducted, are even more weakly stratified. Direct comparison of maximum N^2 to Chl/$b_{bp\_ESP\_avg}$ suggests that weak stratification is a prerequisite for detecting recent eddy subduction (Supporting Information Figure S5). Interestingly, despite its strong seasonality, mixed layer depth does not show much effect – distributions are similar between profiles with and without subduction anomalies (Figure 4e). Conversely, although FSLEs do not show seasonality, profiles with subduction anomalies are strongly shifted towards stronger nearby FSLEs, implying closer proximity to strong lateral buoyancy gradients (Figure 4f).

These statistical analyses indicate that in the Southern Ocean, strong lateral buoyancy gradients and weak vertical stratification exert significant physical controls on eddy subduction. The spatial analyses in Section 3.1 suggest that these mechanisms drive eddy subduction's concentration in standing meanders and weakly stratified areas. Meanwhile, the seasonal analyses in Sections 3.2 and 3.3 suggest that vertical stratification is the dominant driver of seasonality, along with the seasonal availability of surface POC. Mixed layer depth appears to exert little influence. Thus, in areas prone to submesoscale motions, weak springtime stratification may act as a seasonal trapdoor that determines whether they can export material beneath the mixed layer. Indeed, this is consistent with Stommel's Demon, which argues that a "demon" selects the properties of late winter water to be injected into the ocean interior (Stommel, 1979).

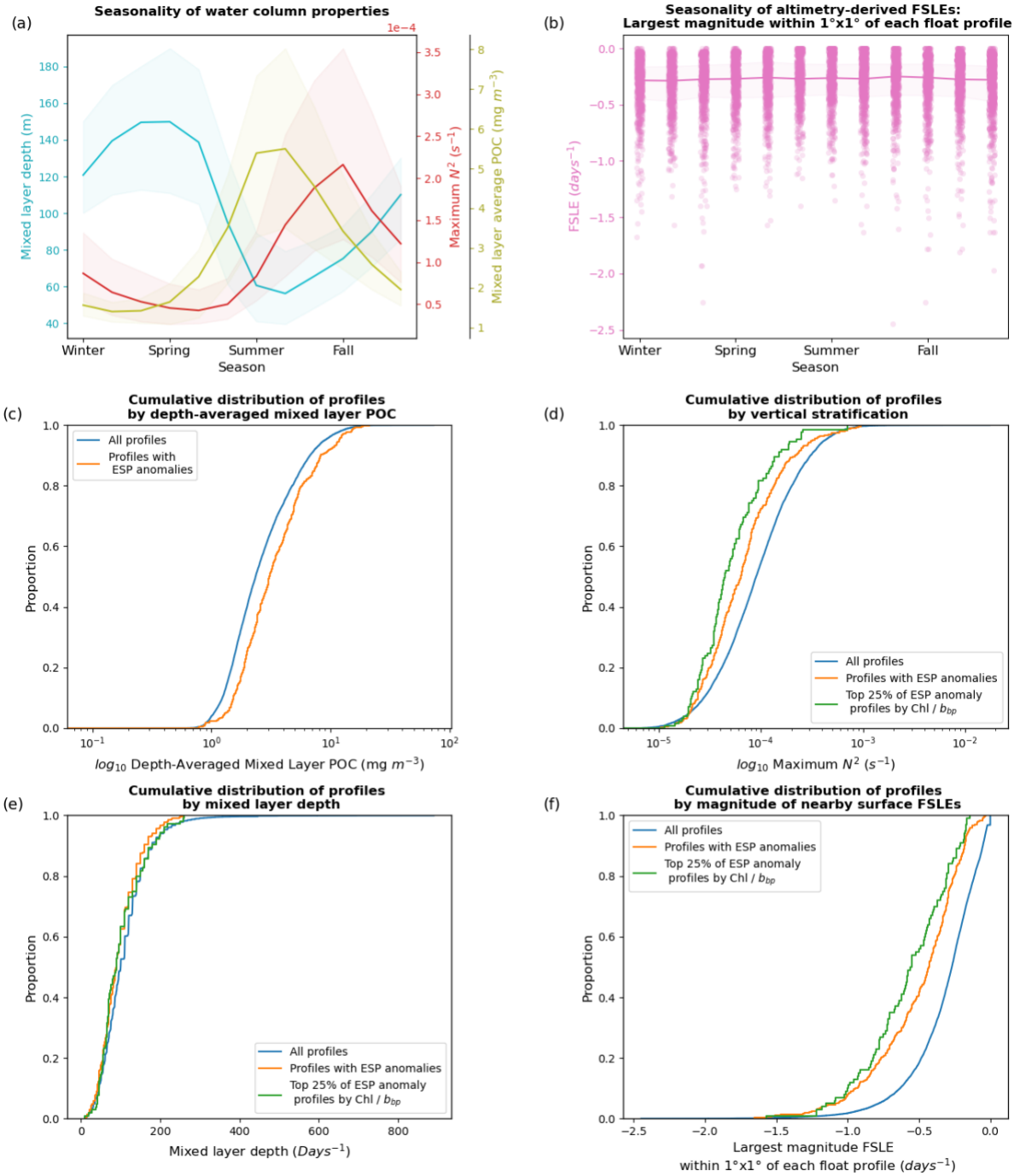

Figure 4. Mechanisms driving eddy subduction. **(a)** Seasonality of water column properties for all float profiles, showing MLD (blue), maximum N^2 (red), and depth-averaged POC within the surface mixed layer (olive). The line plot depicts medians, with shaded regions indicating interquartile ranges. **(b)** Seasonality of altimetry-derived FSLE magnitudes. The strip plot shows satellite matchups to each float profile, showing the strongest FSLE within 1°x1°. Line plot as in **(a).** **(c-f)** Cumulative distribution plots of profiles by various mechanistic variables. Each curve represents the cumulative proportion of observations falling below the corresponding x-axis

value. Colors indicate all profiles (blue), only profiles with ESP anomalies (orange), and only profiles with ESP anomalies with the highest 25% Chl/$b_{bp\_ESP\_avg}$ values (green) **(c)** Depth-averaged mixed layer POC (log_{10}) **(d)** Maximum N^2 (log_{10}). **(e)** Mixed layer depth. **(f)** Magnitude of the strongest altimetry-derived FSLE within a 1°x1° area.

5 Conclusions

Our work has several broad implications for our understanding of carbon export and submesoscale dynamics, and emphasizes open questions for the community. First, we find evidence of a seasonal cycle in eddy subduction, which has remained unresolved in global carbon export calculations (Nowicki et al., 2022). Future work should assess global variability in regions beyond the Southern Ocean. Second, we highlight the utility of bio-optical proxies such as Chl/b_{bp} ratios beneath the ocean's surface. However, high-resolution sampling is necessary to quantify the evolution and aging of tracers over the course of submesoscale processes. Third, we emphasize the power of contextualizing subsurface float observations with Lagrangian diagnostics from satellites such as FSLEs. Finally, we identify strong lateral buoyancy gradients and weak vertical stratification as key spatiotemporal controls on vertical exchange in the Southern Ocean. Future investigation should untangle specific physical mechanisms and the relative impacts of frontogenesis versus instabilities (Archer et al., 2020; Callies et al., 2015; Erickson & Thompson, 2018; Klein & Lapeyre, 2009; Rosso et al., 2015). Finally, climate change has been driving increased stratification strength across global oceans (Sallée et al., 2021), potentially decreasing eddy subduction's contribution to global carbon export.

Acknowledgments

The authors are grateful for conversations with Joan Llort, Shuangling Chen, Léo Lacour, Laure Resplandy, Kathleen Abbott, Lily Dove, Mara Freilich, and Jackie Veatch. Float data were collected and made freely available by the SOCCOM Project funded by the National Science Foundation, Division of Polar Programs (NSF PLR -1425989 and OPP-1936222), supplemented by NASA, and by the International Argo Program and the NOAA programs that contribute to it. The Argo Program is part of the Global Ocean Observing System. M.L. Chen acknowledges NASA Grant 80NSSC22K1451. O. Schofield acknowledges NASA Grant 80NSSC21K0969.

Open Research

Float data were downloaded from the UCSD SOCCOM and GO-BGC data archive. Our analyses use the delayed-mode, quality controlled, low-resolution snapshot from 2023-08-28 (Riser et al., 2023). Altimetry-derived FSLEs were produced by Ssalto/Duacs in collaboration with LOcean and CTOH and distributed by AVISO+, with support from CNES (https://www.aviso.altimetry.fr/en/data/products/value-added-products/fsle-finite-size-lyapunov-exponents.html). Analyses were conducted in Python 3.8.17 using Xarray version 2022.11.0, available under the Apache license at https://docs.xarray.dev/ (The Xarray Development Team, 2022); GSW version 3.6.17, available under the GSW License at https://www.TEOS-10.org (McDougall & Barker, 2011); and Pandas version 1.5.3, available under the BSD 3-Clause "New" or "Revised" License at https://pandas.pydata.org (The Pandas Development, 2023).

Figures were plotted using Matplotlib version 3.7.1, available under the Matplotlib license at https://matplotlib.org (The Matplotlib Development Team, 2023); Seaborn version 0.12, available under the BSD 3-Clause "New" or "Revised" License at https://seaborn.pydata.org (The Seaborn Development Team, 2022); and Cartopy version 0.21.1, available under the BSD-3 Clause License at https://scitools.org.uk/cartopy/) (The Cartopy Development Team, 2022). The software associated with this manuscript for data processing and analysis is licensed under MIT and published on GitHub https://github.com/mchen96/southern_ocean_eddy_subduction/, and can be run in a zero-install environment on the cloud at https://mybinder.org/v2/gh/mchen96/southern_ocean_eddy_subduction/main (Chen, 2024).

References

Archer, M., Schaeffer, A., Keating, S., Roughan, M., Holmes, R., & Siegelman, L. (2020). Observations of Submesoscale Variability and Frontal Subduction within the Mesoscale Eddy Field of the Tasman Sea. *Journal of Physical Oceanography*, *50*(5), 1509–1529. https://doi.org/10.1175/JPO-D-19-0131.1

Balwada, D., Smith, K. S., & Abernathey, R. (2018). Submesoscale Vertical Velocities Enhance Tracer Subduction in an Idealized Antarctic Circumpolar Current. *Geophysical Research Letters*, *45*(18), 9790–9802. https://doi.org/10.1029/2018GL079244

Barbieux, M., Uitz, J., Bricaud, A., Organelli, E., Poteau, A., Schmechtig, C., et al. (2018). Assessing the Variability in the Relationship Between the Particulate Backscattering Coefficient and the Chlorophyll *a* Concentration From a Global Biogeochemical-Argo Database. *Journal of Geophysical Research: Oceans*, *123*(2), 1229–1250. https://doi.org/10.1002/2017JC013030

Bianchi, D., Stock, C., Galbraith, E. D., & Sarmiento, J. L. (2013). Diel vertical migration: Ecological controls and impacts on the biological pump in a one-dimensional ocean model. *Global Biogeochemical Cycles*, *27*(2), 478–491. https://doi.org/10.1002/gbc.20031

Boccaletti, G., Ferrari, R., & Fox-Kemper, B. (2007). Mixed Layer Instabilities and Restratification. *Journal of Physical Oceanography*, *37*(9), 2228–2250. https://doi.org/10.1175/JPO3101.1

Boyd, P. W., Claustre, H., Levy, M., Siegel, D. A., & Weber, T. (2019). Multi-faceted particle pumps drive carbon sequestration in the ocean. *Nature*, *568*(7752), 327–335. https://doi.org/10.1038/s41586-019-1098-2

Briggs, N., Perry, M. J., Cetinić, I., Lee, C., D'Asaro, E., Gray, A. M., & Rehm, E. (2011). High-resolution observations of aggregate flux during a sub-polar North Atlantic spring bloom. *Deep Sea Research Part I: Oceanographic Research Papers*, *58*(10), 1031–1039. https://doi.org/10.1016/j.dsr.2011.07.007

Buckingham, C. E., Naveira Garabato, A. C., Thompson, A. F., Brannigan, L., Lazar, A., Marshall, D. P., et al. (2016). Seasonality of submesoscale flows in the ocean surface boundary layer. *Geophysical Research Letters*, *43*(5), 2118–2126. https://doi.org/10.1002/2016GL068009

Callies, J., Ferrari, R., Klymak, J. M., & Gula, J. (2015). Seasonality in submesoscale turbulence. *Nature Communications*, *6*(1), 6862. https://doi.org/10.1038/ncomms7862

Callies, J., Flierl, G., Ferrari, R., & Fox-Kemper, B. (2016). The role of mixed-layer instabilities in submesoscale turbulence. *Journal of Fluid Mechanics*, *788*, 5–41. https://doi.org/10.1017/jfm.2015.700

Capet, X., McWilliams, J. C., Molemaker, M. J., & Shchepetkin, A. F. (2008). Mesoscale to Submesoscale Transition in the California Current System. Part I: Flow Structure, Eddy Flux, and Observational Tests. *Journal of Physical Oceanography*, *38*(1), 29–43. https://doi.org/10.1175/2007JPO3671.1

Cetinić, I., Perry, M. J., D'Asaro, E., Briggs, N., Poulton, N., Sieracki, M. E., & Lee, C. M. (2015). A simple optical index shows spatial and temporal heterogeneity in phytoplankton community composition during the 2008 North Atlantic Bloom Experiment. *Biogeosciences*, *12*(7), 2179–2194. https://doi.org/10.5194/bg-12-2179-2015

Chen, M. (2024, April 24). Southern Ocean Eddy Subduction (Version v1.0.2). [software]. Zenodo. https://doi.org/10.5281/ZENODO.11062305

Chen, S., Wells, M. L., Huang, R. X., Xue, H., Xi, J., & Chai, F. (2021). Episodic subduction patches in the western North Pacific identified from BGC-Argo float data. *Biogeosciences*, *18*(19), 5539–5554. https://doi.org/10.5194/bg-18-5539-2021

Dall'Olmo, G., Dingle, J., Polimene, L., Brewin, R. J. W., & Claustre, H. (2016). Substantial energy input to the mesopelagic ecosystem from the seasonal mixed-layer pump. *Nature Geoscience*, *9*(11), 820–823. https://doi.org/10.1038/ngeo2818

Davies, A. R., Veron, F., & Oliver, M. J. (2019). Biofloat observations of a phytoplankton bloom and carbon export in the Drake Passage. *Deep Sea Research Part I: Oceanographic Research Papers*, *146*, 91–102. https://doi.org/10.1016/j.dsr.2019.02.004

Dove, L. A., Balwada, D., Thompson, A. F., & Gray, A. R. (2022). Enhanced Ventilation in Energetic Regions of the Antarctic Circumpolar Current. *Geophysical Research Letters*, *49*(13), e2021GL097574. https://doi.org/10.1029/2021GL097574

Erickson, Z. K., & Thompson, A. F. (2018). The Seasonality of Physically Driven Export at Submesoscales in the Northeast Atlantic Ocean. *Global Biogeochemical Cycles*. https://doi.org/10.1029/2018GB005927

Fox-Kemper, B., Ferrari, R., & Hallberg, R. (2008). Parameterization of Mixed Layer Eddies. Part I: Theory and Diagnosis. *Journal of Physical Oceanography*, *38*(6), 1145–1165. https://doi.org/10.1175/2007JPO3792.1

Garcia, H. E., & Gordon, L. I. (1992). Oxygen solubility in seawater: Better fitting equations. *Limnology and Oceanography*, *37*(6), 1307–1312. https://doi.org/10.4319/lo.1992.37.6.1307

Garcia, H. E., & Gordon, L. I. (1993). Erratum: Oxygen solubility in seawater: Better fitting equations. *Limnology and Oceanography*, *38*, 656.

Gruber, N., Gloor, M., Mikaloff Fletcher, S. E., Doney, S. C., Dutkiewicz, S., Follows, M. J., et al. (2009). Oceanic sources, sinks, and transport of atmospheric CO2. *Global Biogeochemical Cycles*, *23*(1), n/a-n/a. https://doi.org/10.1029/2008GB003349

Held, I. M., Pierrehumbert, R. T., Garner, S. T., & Swanson, K. L. (1995). Surface quasi-geostrophic dynamics. *Journal of Fluid Mechanics*, *282*, 1–20. https://doi.org/10.1017/S0022112095000012

Johnson, A. R., & Omand, M. M. (2021). Evolution of a Subducted Carbon-Rich Filament on the Edge of the North Atlantic Gyre. *Journal of Geophysical Research: Oceans*, *126*(2). https://doi.org/10.1029/2020JC016685

Johnson, K. S., Plant, J. N., Coletti, L. J., Jannasch, H. W., Sakamoto, C. M., Riser, S. C., et al. (2017). Biogeochemical sensor performance in the SOCCOM profiling float array. *Journal of Geophysical Research: Oceans*, *122*(8), 6416–6436. https://doi.org/10.1002/2017JC012838

Klein, P., & Lapeyre, G. (2009). The Oceanic Vertical Pump Induced by Mesoscale and Submesoscale Turbulence. *Annual Review of Marine Science*, *1*(1), 351–375. https://doi.org/10.1146/annurev.marine.010908.163704

Lacour, L., Briggs, N., Claustre, H., Ardyna, M., & Dall'Olmo, G. (2019). The Intraseasonal Dynamics of the Mixed Layer Pump in the Subpolar North Atlantic Ocean: A Biogeochemical-Argo Float Approach. *Global Biogeochemical Cycles*, *33*(3), 266–281. https://doi.org/10.1029/2018GB005997

Lacour, Léo, Llort, J., Briggs, N., Strutton, P. G., & Boyd, P. W. (2023). Seasonality of downward carbon export in the Pacific Southern Ocean revealed by multi-year robotic observations. *Nature Communications*, *14*(1), 1278. https://doi.org/10.1038/s41467-023-36954-7

Lapeyre, G., & Klein, P. (2006). Dynamics of the Upper Oceanic Layers in Terms of Surface Quasigeostrophy Theory. *Journal of Physical Oceanography*, *36*(2), 165–176. https://doi.org/10.1175/JPO2840.1

Lévy, M., Ferrari, R., Franks, P. J. S., Martin, A. P., & Rivière, P. (2012). Bringing physics to life at the submesoscale. *Geophysical Research Letters*, *39*(14), 2012GL052756. https://doi.org/10.1029/2012GL052756

Levy, M., Bopp, L., Karleskind, P., Resplandy, L., Ethe, C., & Pinsard, F. (2013). Physical pathways for carbon transfers between the surface mixed layer and the ocean interior. *Global Biogeochemical Cycles*, *27*(4), 1001–1012. https://doi.org/10.1002/gbc.20092

Llort, J., Langlais, C., Matear, R., Moreau, S., Lenton, A., & Strutton, P. G. (2018). Evaluating Southern Ocean Carbon Eddy-Pump From Biogeochemical-Argo Floats. *Journal of Geophysical Research: Oceans*, *123*(2), 971–984. https://doi.org/10.1002/2017JC012861

Mahadevan, A., & Tandon, A. (2006). An analysis of mechanisms for submesoscale vertical motion at ocean fronts. *Ocean Modelling*, *14*(3–4), 241–256. https://doi.org/10.1016/j.ocemod.2006.05.006

Maurer, T. L., Plant, J. N., & Johnson, K. S. (2021). Delayed-Mode Quality Control of Oxygen, Nitrate, and pH Data on SOCCOM Biogeochemical Profiling Floats. *Frontiers in Marine Science*, *8*, 683207. https://doi.org/10.3389/fmars.2021.683207

McDougall, T. J., & Barker, P. M. (2011). Getting started with TEOS-10 and the Gibbs seawater (GSW) oceanographic toolbox. *SCOR/IAPSO WG*, *127*, 1–28.

McDougall, T. J., & Krzysik, O. A. (2015). Spiciness. *Journal of Marine Research*, *73*(5), 141–152. https://doi.org/10.1357/002224015816665589

Nowicki, M., DeVries, T., & Siegel, D. A. (2022). Quantifying the Carbon Export and Sequestration Pathways of the Ocean's Biological Carbon Pump. *Global Biogeochemical Cycles*, *36*(3), e2021GB007083. https://doi.org/10.1029/2021GB007083

Omand, M. M., D'Asaro, E. A., Lee, C. M., Perry, M. J., Briggs, N., Cetinić, I., & Mahadevan, A. (2015). Eddy-driven subduction exports particulate organic carbon from the spring bloom. *Science*, *348*(6231), 222–225. https://doi.org/10.1126/science.1260062

d'Ovidio, F., Fernández, V., Hernández-García, E., & López, C. (2004). Mixing structures in the Mediterranean Sea from finite-size Lyapunov exponents. *Geophysical Research Letters*, *31*(17), 2004GL020328. https://doi.org/10.1029/2004GL020328

Park, Y.-H., & Durand, I. (2019). Altimetry-drived Antarctic Circumpolar Current fronts [Data set]. SEANOE. https://doi.org/10.17882/59800

Rembauville, M., Briggs, N., Ardyna, M., Uitz, J., Catala, P., Penkerc'h, C., et al. (2017). Plankton Assemblage Estimated with BGC-Argo Floats in the Southern Ocean: Implications for Seasonal Successions and Particle Export: PLANKTON ASSEMBLAGE BGC-ARGO. *Journal of Geophysical Research: Oceans*, *122*(10), 8278–8292. https://doi.org/10.1002/2017JC013067

Resplandy, L., Lévy, M., & McGillicuddy, D. J. (2019). Effects of Eddy-Driven Subduction on Ocean Biological Carbon Pump. *Global Biogeochemical Cycles*, *33*(8), 1071–1084. https://doi.org/10.1029/2018GB006125

Riser, S. C., Talley, L. D., Wijffels, S. E., Nicholson, D., Purkey, S., Takeshita, Y., et al. (2023). Southern Ocean Carbon and Climate Observations and Modeling (SOCCOM) and Global Ocean Biogeochemistry (GO-BGC) Biogeochemical-Argo Float Data Archive [Data set]. UC San Diego Library Digital Collections. https://doi.org/10.6075/J0SJ1KT8

Rosso, I., Hogg, A. McC., Strutton, P. G., Kiss, A. E., Matear, R., Klocker, A., & Van Sebille, E. (2014). Vertical transport in the ocean due to sub-mesoscale structures: Impacts in the Kerguelen region. *Ocean Modelling*, *80*, 10–23. https://doi.org/10.1016/j.ocemod.2014.05.001

Rosso, I., Hogg, A. McC., Kiss, A. E., & Gayen, B. (2015). Topographic influence on submesoscale dynamics in the Southern Ocean. *Geophysical Research Letters*, *42*(4), 1139–1147. https://doi.org/10.1002/2014GL062720

Sallée, J.-B., Pellichero, V., Akhoudas, C., Pauthenet, E., Vignes, L., Schmidtko, S., et al. (2021). Summertime increases in upper-ocean stratification and mixed-layer depth. *Nature*, *591*(7851), 592–598. https://doi.org/10.1038/s41586-021-03303-x

Siegelman, L., Klein, P., Thompson, A. F., Torres, H. S., & Menemenlis, D. (2020a). Altimetry-Based Diagnosis of Deep-Reaching Sub-Mesoscale Ocean Fronts. *Fluids*, *5*(3), 145. https://doi.org/10.3390/fluids5030145

Siegelman, L., Klein, P., Rivière, P., Thompson, A. F., Torres, H. S., Flexas, M., & Menemenlis, D. (2020b). Enhanced upward heat transport at deep submesoscale ocean fronts. *Nature Geoscience*, *13*(1), 50–55. https://doi.org/10.1038/s41561-019-0489-1

Stommel, H. (1979). Determination of water mass properties of water pumped down from the Ekman layer to the geostrophic flow below. *Proceedings of the National Academy of Sciences*, *76*(7), 3051–3055. https://doi.org/10.1073/pnas.76.7.3051

Stukel, M. R., & Ducklow, H. W. (2017). Stirring Up the Biological Pump: Vertical Mixing and Carbon Export in the Southern Ocean: Vertical Mixing and Carbon Export in SO. *Global Biogeochemical Cycles*, *31*(9), 1420–1434. https://doi.org/10.1002/2017GB005652

Tailleux, R. (2021). Spiciness theory revisited, with new views on neutral density, orthogonality, and passiveness. *Ocean Science*, *17*(1), 203–219. https://doi.org/10.5194/os-17-203-2021

The Matplotlib Development Team. (2023, March 4). Matplotlib (Version v3.7.1). [software]. Zenodo. https://doi.org/10.5281/ZENODO.7697899

The Pandas Development. (2023, January 19). Pandas (Version v1.5.3). [software]. Zenodo. https://doi.org/10.5281/ZENODO.7549438

The Seaborn Development Team. (2022, December 30). Seaborn (Version v0.12.2). [software]. Zenodo. https://doi.org/10.5281/ZENODO.7495530

The Xarray Development Team. (2022, October 13). xarray (Version v2022.10.0). [software]. Zenodo. https://doi.org/10.5281/ZENODO.7195919

Thompson, A. F., Lazar, A., Buckingham, C., Naveira Garabato, A. C., Damerell, G. M., & Heywood, K. J. (2016). Open-Ocean Submesoscale Motions: A Full Seasonal Cycle of Mixed Layer Instabilities from Gliders. *Journal of Physical Oceanography*, *46*(4), 1285–1307. https://doi.org/10.1175/JPO-D-15-0170.1